THE JOURNAL OF PHYSICAL CHEMISTRY Letters

ACS Editors' Choice

Letter

pubs.acs.org/JPCL

Terms of Use

Parameters Affecting *I*–*V* Hysteresis of $CH_3NH_3PbI_3$ Perovskite Solar Cells: Effects of Perovskite Crystal Size and Mesoporous TiO_2 Layer

Hui-Seon Kim and Nam-Gyu Park*

School of Chemical Engineering and Department of Energy Science, Sungkyunkwan University (SKKU), 300 Cheoncheon-dong, Jangan-gu, Suwon 440-746, Korea

Supporting Information

ABSTRACT: Current–voltage (*I*–*V*) characteristics of $CH_3NH_3PbI_3$ perovskite solar cells are studied using a time-dependent current response with stepwise sweeping of the bias voltage. Compared with the crystalline Si solar cell showing time-independent current at a given bias voltage, the perovskite solar cells exhibit time-dependent current response. The current increases with time and becomes steady at forward scan from short-circuit to open-circuit, whereas it is decayed and saturated with time at reverse scan from open-circuit to short-circuit. Time-dependent current response eventually leads to *I*–*V* hysteresis depending on the scan direction and the scan rate. Crystal size of $CH_3NH_3PbI_3$ and the mesoporous TiO_2 (mp-TiO_2) film are found to influence *I*–*V* hysteresis, where the *I*–*V* hysteresis is alleviated as crystal size increases and in the presence of mp-TiO_2. The capacitance observed at low frequency (0.1 to 1 Hz), associated with dipole polarization, tends to diminish as size of perovskite and mp-TiO_2 layer thickness increases, which suggests that the origin of hysteresis correlates to the capacitive characteristic of $CH_3NH_3PbI_3$ and the degree of hysteresis depends strongly on perovskite crystal size and mesoporous TiO_2 layer.

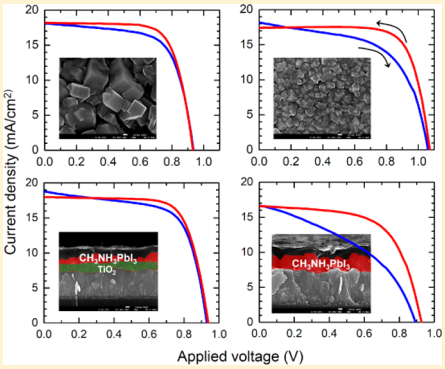

SECTION: Energy Conversion and Storage; Energy and Charge Transport

Since organometal halide perovskite (ABX_3, X = halide) has been introduced into solid-state semiconductor-sensitized solar cell showing a high efficiency of ~10% in 2012,[1,2] it has attracted great interest and eventually led the paradigm shift in photovoltaic technology. At the beginning, $CH_3NH_3PbI_3$ perovskite was regarded as a light absorber having a high absorption coefficient that enables 0.6 μm thick TiO_2 film to demonstrate power conversion efficiency (PCE) of 9.7% under A.M. 1.5 G one sun illumination with a current density of 17.6 mA/cm^2.[1] Snaith et al. reported that $CH_3NH_3PbI_2Cl$ deposited onto Al_2O_3 porous film showed a PCE of 10.9%, where hole was separated to a hole transporting layer (HTL) and electron was transported in the extremely thin perovskite layer covered on the scaffold Al_2O_3 surface.[2] A surge of attention has been paid because in a very short period PCE of perovskite solar cell rapidly increased up to ~15% by modifying perovskite deposition method from one-step solution coating to sequential two-step coating[3] and vapor evaporation.[4] Also, more facile method for the preparation of planar and uniformed perovskite layer with large grain size (~500 nm) was developed by aid of $CH_3NH_3PbI_3$ vapor deposition over the PbI_2 substrate.[5] Recently, a certified PCE of 17.9% appeared in a 'Best Research-Cell Efficiency' table updated by the national renewable energy laboratory (NREL). Although perovskite solar cells show superb photovoltaic performance, perovskite materials possess some weak points such as instability against humidity and UV light[6,7] and lead to toxicity as well. While the instability of the perovskite to humidity is very well known, instability to UV is not so obvious. Because it was reported that there was instability to light absorbed by TiO_2,[7] instability to UV may not be an intrinsic property of the perovskite. To complement these drawbacks, many attempts have been tried by mixing bromide and iodide,[8] surface modification of TiO_2 with Sb_2S_3,[6] modifying oxide nanostructure,[7] and substituting Pb with Sn.[9−11]

In parallel with achieving high efficiency and developing beneficial process, many attempts to understand fundamental working principle of the perovskite solar cell have been made based on impedance spectroscopy (IS),[12−16] transient photovoltage and photocurrent,[17,18] femtosecond transient optical spectroscopy,[19,20] and theoretical calculation.[21,22] Meanwhile, little attention has been paid to the hysteresis behavior of perovskite solar cells. Anomalous *I*–*V* hysteresis was recently observed from the mixed halide perovskite $CH_3NH_3PbI_{3-x}Cl_x$,[23] where *I*–*V* hysteresis was found to be significantly dependent on the p- and n-type contact materials and mesoporous versus planar structures. Defects and polarization were hypothesized for the origin of the *I*–*V* hysteresis. To scrutinize the origin of the *I*–*V* hysteresis, factors affecting the hysteresis are needed to be further investigated. Here we

Received: July 4, 2014
Accepted: August 11, 2014
Published: August 11, 2014

   dx.doi.org/10.1021/jz501392m | *J. Phys. Chem. Lett.* 2014, 5, 2927–2934

report on the factors affecting the $I-V$ hysteresis of $CH_3NH_3PbI_3$ perovskite solar cell, which can provide important insight into not only unraveling but also attenuating the $I-V$ hysteresis. Effects of $CH_3NH_3PbI_3$ crystal size and mesoporous TiO_2 layer thickness on the hysteresis are investigated. IS studies are performed to understand the origin of the hysteresis.

Capacitive characteristics in solar cells can affect the period to reach the steady-state condition, which leads to the $I-V$ hysteresis. Thus, the degree of the hysteresis depends principally on the voltage settling time (waiting period to measure current after applying a given voltage). In the case of Si solar cell, its capacitance in the range of $\mu F/cm^2$ makes optimal voltage settling time for $I-V$ measurement as 10 ms,[24] whereas dye-sensitized solar cell showing three orders of higher capacitance (mF/cm^2) should be measured at voltage settling time longer than 40 ms.[25] Considering the fact that the semiconductor $CH_3NH_3PbI_3$-sensitized cell[12] exhibits more than two orders of magnitude higher capacitive character than the dye-sensitized one, perovskite solar cell is assumed to show severe $I-V$ hysteresis compared with the Si solar cell.

Figure 1a shows $I-V$ curves of monocrystalline Si solar cell obtained from forward scan (from short-circuit to open-circuit

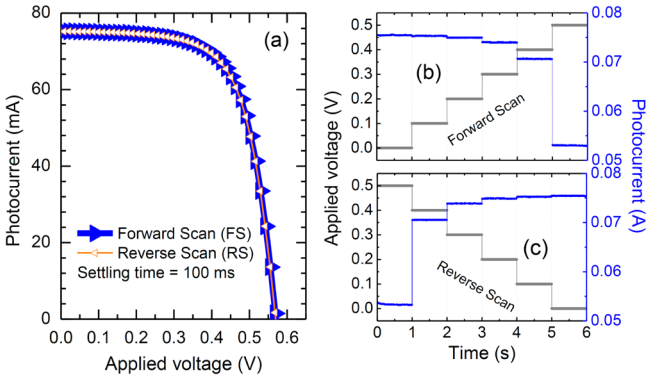

Figure 1. (a) $I-V$ curves of Si solar cell at forward scan (FS) and reverse scan (RS). Thick blue line with filled triangles and thin red line with open triangles represent FS and RS, respectively. Time-dependent photocurrent response of Si solar cell as a function of voltage settling time at (b) FS and (c) RS.

under the forward bias voltage, hereafter abbreviated as FS) and reverse scan (from open-circuit to short-circuit under the forward bias voltage, hereafter abbreviated as RS) at the voltage settling time of 100 ms. As expected, little difference between $I-V$ curves is observed regardless of sweep direction. We also confirm that $I-V$ curves are hardly dependent on the settling time ranging from 10 to 500 ms. (Data are not shown.) The time-dependent current response of Si solar cell is measured by a linear stepwise voltage sweep, where time for each step is given as 1 s and the resulting current is detected every 0.001 s, as shown in Figure 1b,c. Figure 1b shows the time-dependent current at FS, and Figure 1c shows the time-dependent current at RS. It is found that the current response is sufficiently rapid and reaches its saturation point within 0.001 s for both directions, leading to a time-independent current response, which is responsible for almost no $I-V$ hysteresis, as observed in Figure 1a.

First, effects of perovskite crystal size on $I-V$ hysteresis and time-dependent photocurrent response are investigated. Figure 2a–c shows surface SEM images of different $CH_3NH_3PbI_3$ crystal size. The crystal size is controlled by varying concentration of the CH_3NH_3I solution in the two-step spin-coating method. A large crystal is expected from the low concentration of CH_3NH_3I solution because the slow crystal growth occurs over a longer period of time in low concentration, whereas a small crystal is grown in the high concentration of CH_3NH_3I because a large number of crystals are already developed in the very beginning and their simultaneous growth inhibits the large size of crystal. As can be seen in the SEM images, crystal size increases from 130 to 170 nm and to 440 nm as the CH_3NH_3I solution concentration decreases from 62.91 to 52.42 mM and to 41.94 mM, respectively. It is found that open-circuit voltage (V_{oc}) increases with decreasing the perovskite size (Figure 2 and Table 1). Dark $I-V$ (Figure S1 in the Supporting Information) shows that dark current decreases with decreasing the size, which indicates that the enhancement of V_{oc} with small crystal size is caused by its compact crystal morphology preventing HTM from direct contact with TiO_2 or FTO. However, correlation between V_{oc} and capacitive effect cannot be ruled out, which will be discussed afterward. Figure 2d–f shows the scan-direction-dependent $I-V$ curves. It is noted that $I-V$ hysteresis becomes more pronounced as the size decreases. For the case of 130 nm sized perovskite, photocurrent density continuously decreases with the applied bias voltage especially at FS, leading to worse fill factor (FF) at FS compared with the RS case, as shown in Figure 2f. Relatively little difference in FF between FS and RS is observed, even for a slight increase in size from 130 to 170 nm (Figure 2e). Because the prominent feature in the $I-V$ hysteresis appears near open-circuit condition, a modified $I-V$ hysteresis index[26] is defined by eq 1

$$\text{hysteresis index} = \frac{J_{RS}(0.8V_{oc}) - J_{FS}(0.8V_{oc})}{J_{RS}(0.8V_{oc})} \quad (1)$$

where $J_{RS}(0.8V_{oc})$ and $J_{FS}(0.8V_{oc})$ represent photocurrent density at 80% of V_{oc} for the RS and FS, respectively. In Table 1, hysteresis index values are listed together with photovoltaic parameters depending on scan direction. At the given voltage settling time of 200 ms, small size of 130 nm shows large hysteresis index of 0.212 compared with larger sizes, and little difference in hysteresis index is observed between 170 and 440 nm, which indicates that the $CH_3NH_3PbI_3$ size smaller than 170 nm may cause severe hysteresis. Similar tendency is observed at different voltage settling time such as 100 or 500 ms. (Data are not shown.)

To investigate dynamic property of $CH_3NH_3PbI_3$ perovskite solar cell, we measured a time-dependent photocurrent response as shown in Figures 3 and 4. A staircase voltage sweep is made to perovskite solar cells where voltage applying time for each step is given as 5 s, and the resulting current is read every 0.01 s. For example, Figure 3a,c shows overall time-dependent photocurrent response at FS and RS. (The device based on 130 nm sized $CH_3NH_3PbI_3$ is used as an example here.) Figure 3b,d shows the time-dependent photocurrent profile for 5000 ms at a given bias voltage of 0.6 V, as shown in the dotted square box in Figure 3a,c. Contrary to the silicon solar cell, perovskite solar cell shows time-dependent photocurrent. Photocurrent increases exponentially with time and then becomes constant at FS (Figure 3c), while photocurrent is exponentially decayed and invariant with time at RS (Figure 3d). Measurement with the voltage settling time <100 ms can lead to inaccurate $I-V$ data. A strong time-dependent

dx.doi.org/10.1021/jz501392m | J. Phys. Chem. Lett. 2014, 5, 2927–2934

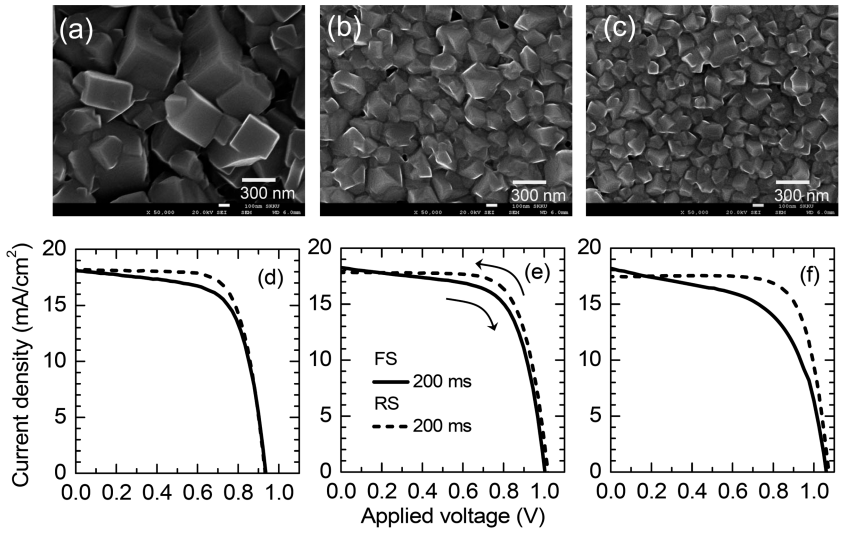

Figure 2. SEM images of $CH_3NH_3PbI_3$ perovskite grown in two-step spin coating procedure with different CH_3NH_3I concentration of (a) 41.94, (b) 52.42, and (c) 62.91 mM, leading to average dimension of 440, 170, and 130 nm, respectively. $I-V$ curves measured at FS (solid line) and RS (dashed line) for the perovskite solar cell employing $CH_3NH_3PbI_3$ with size of (d) 440, (e) 170, and (f) 130 nm. The voltage settling time was 200 ms, and light intensity was AM 1.5G one sun (100 mW/cm^2).

Table 1. Photovoltaic Parameters Obtained at Forward Scan (FS) and Reverse Scan (RS)[a]

$CH_3NH_3PbI_3$ crystal size	sweep direction	J_{sc} (mA/cm^2)	V_{oc} (V)	FF	PCE (%)	hysteresis index
440 nm	FS	18.1	0.936	0.66	11.3	0.087
	RS	18.2	0.933	0.72	12.2	
170 nm	FS	18.3	1.004	0.66	12.0	0.080
	RS	17.8	1.019	0.72	13.1	
130 nm	FS	18.2	1.061	0.58	11.2	0.212
	RS	17.4	1.073	0.74	13.9	

[a]Voltage settling time was 200 ms. The active area was 0.126 cm^2. The hysteresis index was calculated by eq 1.

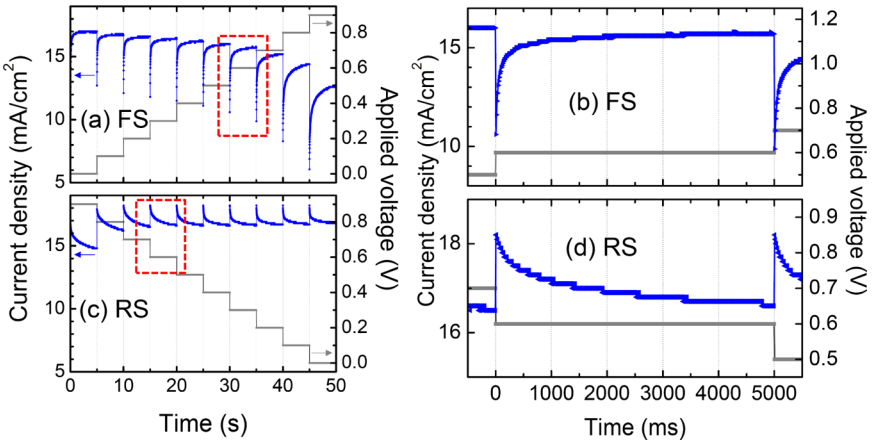

Figure 3. Photocurrent profile depending on time at (a) forward scan (FS) and (c) reverse scan (RS) at stepwise voltage sweep between 0 and 0.9 V. Time-dependent current response at the applied voltage of 0.6 V (shown in dashed-red rectangles) at (b) FS and (d) RS.

photocurrent in ~500 ms at both FS and RS is responsible for the $I-V$ hysteresis of perovskite solar cell. This time-dependent photocurrent response is attributed to the capacitive current (I_c), as defined by eq 2.[27]

$$I_c = C\frac{dV}{dt} + V\frac{dC}{dt} \quad (2)$$

During the voltage sweep, dV/dt is determined by voltage sweep direction (FS or RS) and voltage settling time. I_c has positive or negative value depending on the voltage sweep direction. I_c should be either added or subtracted to or from the non-steady-state photocurrent to compensate the capacitive charge.[27] For example, I_c has a positive value when voltage scan is done from short-circuit to open-circuit direction (FS), and the photogenerated current is accumulated as I_c instead of generating current to external circuit showing underestimated photocurrent density. Enough voltage setting time for steady state, $dV/dt = 0$, is required to avoid storing charge as I_c to get an exact photocurrent density. Thus, in the case of FS, photogenerated current is preferentially stored as capacitive

dx.doi.org/10.1021/jz501392m | J. Phys. Chem. Lett. 2014, 5, 2927−2934

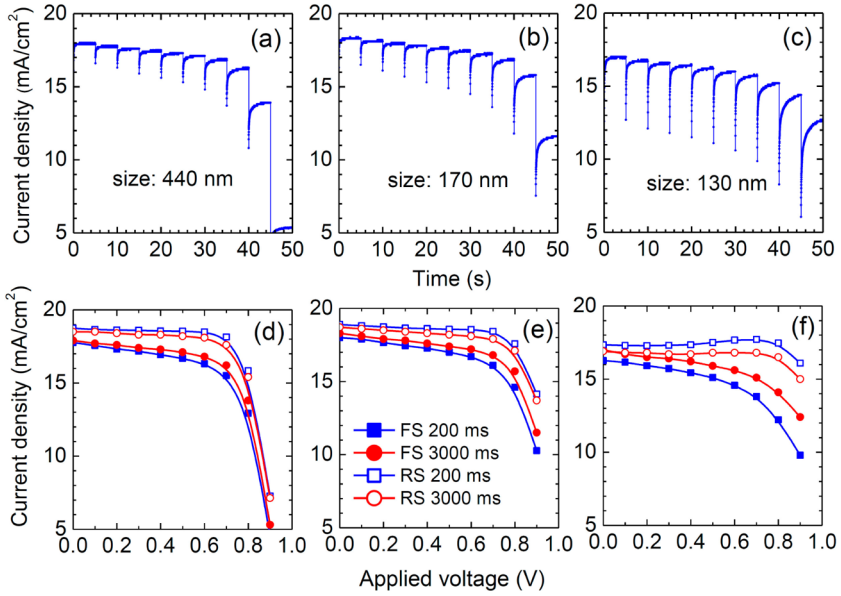

Figure 4. Time-dependent current response of devices depending on $CH_3NH_3PbI_3$ crystal size with (a) 440, (b) 170, and (c) 130 nm at FS. Simulated $I-V$ curves from the time-dependent current data at FS and RS for (d) 440, (e) 170, and (f) 130 nm-sized $CH_3NH_3PbI_3$ crystals, where two different settling times (200 vs 3000 ms) are compared.

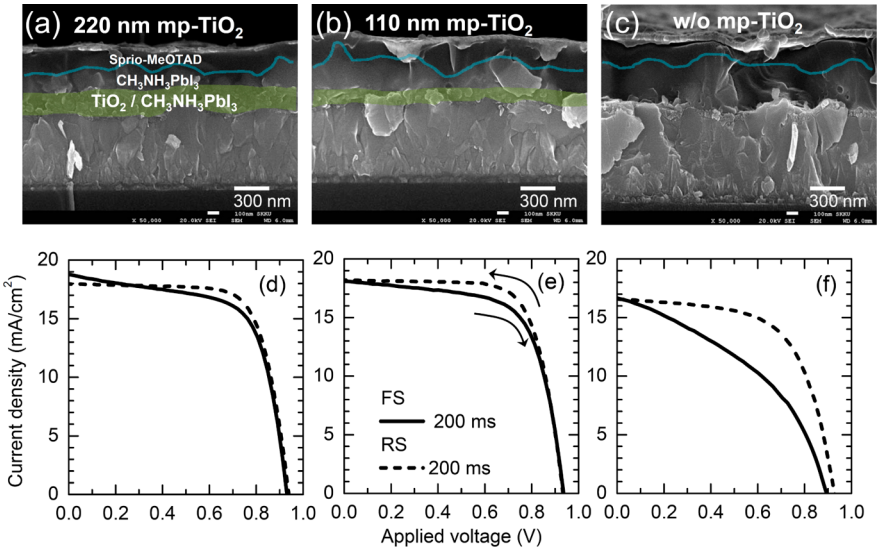

Figure 5. Cross-sectional SEM images of mesostructured devices with (a) 220 and (b) 110 nm thick mp-TiO_2 and (c) planar structured device without mp-TiO_2. $I-V$ curves measured at FS (solid line) and RS (dashed line) for mesostructured devices with (d) 220 and (e) 110 thick mp-TiO_2 and (f) planar structured device without mp-TiO_2. The voltage settling time was 200 ms and light intensity was AM 1.5G one sun (100 mW/cm^2).

charge and thus cannot be extracted toward an external circuit. Conversely, the capacitive charge stored in advance is discharged at RS and collected together with photogenerated current. Therefore, $I-V$ curve shape is significantly dependent on the voltage sweep direction and voltage settling time because the voltage sweep direction decides whether the capacitive charge is accumulated or released and the voltage settling time determines the quantity of capacitive charge to be accumulated or released.

Figure 4 shows overall time-dependent current response depending on the $CH_3NH_3PbI_3$ perovskite crystal size, along with the simulated $I-V$ curves with respect to the settling time. As crystal size decreases from 440 to 130 nm the time-dependent current response becomes clearly intensified, especially at FS, which is responsible for the further aggravation in $I-V$ hysteresis, as shown in Figure 2f. In contrast, the moderate time-dependent current response for the larger size alleviates $I-V$ hysteresis, as shown in Figure 2d. Because photocurrent is more underestimated or overestimated at FS and RS, respectively, as the voltage settling time is shorter, $I-V$ hysteresis is expected to be strongly influenced by the voltage settling time. In Figure 4d–f, $I-V$ curves are simulated in terms of the voltage settling time. As expected, the $I-V$ hysteresis is seen to be alleviated as the voltage settling time increases from 200 to 3000 ms. Such alleviation in the hysteresis at longer settling time is evident as the crystal size decreases. This suggests that small-sized perovskite requires longer time to reach the steady-state photocurrent.

Second, we investigate effect of mesoporous TiO_2 layer on the $I-V$ hysteresis of the $CH_3NH_3PbI_3$ perovskite solar cell.

dx.doi.org/10.1021/jz501392m | J. Phys. Chem. Lett. 2014, 5, 2927−2934

Table 2. Photovoltaic Parameters Obtained at Forward Scan (FS) and Reverse Scan (RS)[a]

mp-TiO_2 thickness	sweep direction	J_{sc} (mA/cm^2)	V_{oc} (V)	FF	PCE (%)	hysteresis index
220 nm	FS	18.4	0.926	0.67	11.5	0.059
	RS	18.5	0.939	0.72	12.5	
110 nm	FS	18.0	0.935	0.68	11.4	0.055
	RS	17.9	0.950	0.72	12.2	
0 nm (planar)	FS	17.1	0.892	0.41	6.3	0.362
	RS	17.1	0.932	0.64	10.2	

[a]Voltage settling time was 200 ms. The active area was 0.126 cm^2. The hysteresis index was calculated by eq 1.

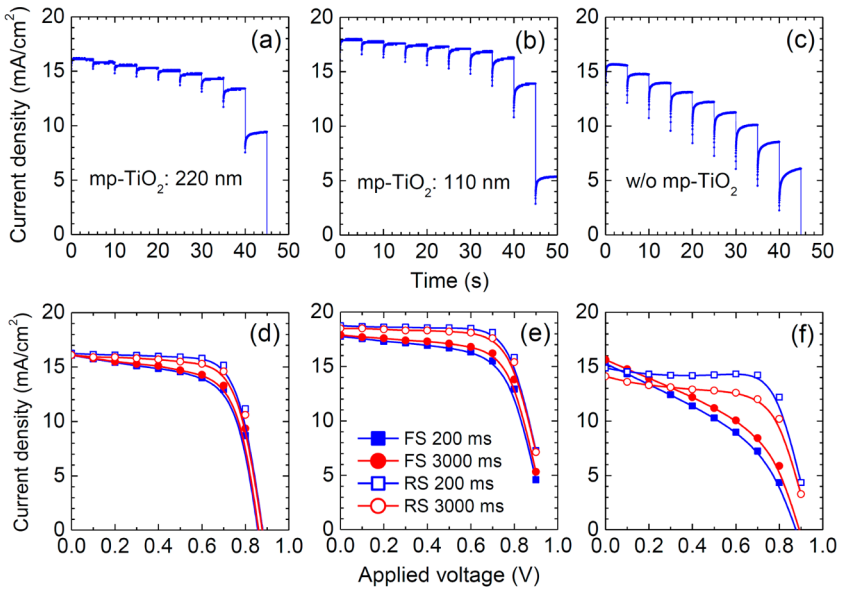

Figure 6. Time-dependent current response of devices with (a) 220 and (b) 110 nm thick mp-TiO_2 and (c) without mp-TiO_2 layer (planar structure) at FS. Simulated $I-V$ curves from the time-dependent current data at FS and RS for devices with (d) 220 and (e) 110 nm thick mp-TiO_2 and (f) without mp-TiO_2 layer (planar structure), where two different settling times (200 vs 3000 ms) are compared.

Figure 5 shows the cross-sectional SEM images of mesostructured devices incorporating mesoporous TiO_2 (mp-TiO_2) films with different thickness of 220 and 110 nm together with a planar structure without mp-TiO_2 and their $I-V$ curves depending on voltage sweep direction at the given settling time of 200 ms. For the crystal size of $CH_3NH_3PbI_3$ used here, 440 nm sized $CH_3NH_3PbI_3$ was prepared by sequential deposition method because it showed the least $I-V$ hysteresis in the previous experiment. It is noted that overall layer thickness of perovskite is almost the same for all devices regardless of mp-TiO_2 film thickness, as shown in Figure 5a–c. Compared with the planar structure without mp-TiO_2 layer, no significant difference in $I-V$ curves between FS and RS is observed for the mesostructured device with mp-TiO_2 layer. This indicates that the mp-TiO_2 layer relives the hysteresis. Severe $I-V$ hysteresis observed from the planar structure is especially due to low FF at FS, which suggests that the capacitive charges to be stored are significantly larger than the mesostructured device with mp-TiO_2 layer. The negligible hysteresis in the presence of mp-TiO_2 layer is likely to be due to the fact that the capacitive charges are quickly dissipated by charge separation. In Table 2, the hysteresis index is estimated to be 0.059, 0.055, and 0.362 for 220 nm thick mp-TiO_2, 110 nm thick mp-TiO_2, and planar structure without mp-TiO_2, which numerically confirms the degree of hysteresis.

To check the dynamic response of $CH_3NH_3PbI_3$ perovskite solar cell depending on the mp-TiO_2 film thickness, the time-dependent current response is also investigated. As can be seen in Figure 6a,b, relatively small negative photocurrents with respect to the steady-state photocurrent are observed at FS for the mp-TiO_2 contained devices, which is reduced as mp-TiO_2 thickness increases. The planar structure shows large negative photocurrents at FS. This confirms that the quantity of capacitive charges is considerably high and the whole photogenerated current is hardly extracted at short settling time without assistance of mp-TiO_2 layer. The simulated $I-V$ curves as a function of the voltage settling time are shown in Figure 6d–f. A negligible dependence of $I-V$ curves on the settling time is evaluated for the perovskite employing mp-TiO_2 layer, while a large difference is obtained from the planar structure. The hysteresis index looks smaller as the voltage setting time increases from 200 to 3000 ms for the planar structure, but still this structure suffers from severe hysteresis. It is certain that mp-TiO_2 has a significant impact on the suppression in the $I-V$ hysteresis, which is also observed elsewhere.[23]

It is reported that $CH_3NH_3PbI_3$ perovskite solar cell shows specific capacitances in intermediate (~656 Hz) and low (~0.28 Hz) frequency ranges, where the former is chemical capacitance (C_μ) due to the electron traps in perovskite material and the latter, low frequency capacitance (C_{LF}), is considered to be the origin of $I-V$ hysteresis in lead halide perovskite solar cell closely related to the relaxation of polarization.[26,28] To investigate the relationship between

dx.doi.org/10.1021/jz501392m | J. Phys. Chem. Lett. 2014, 5, 2927–2934

capacitance and $I-V$ hysteresis, we measured IS at bias voltage of 0.8 V. We select this bias voltage because $I-V$ hysteresis commonly appears evidently at this voltage that is also close to 80% of V_{oc} corresponding to the voltage for hysteresis index evaluation. In Figure 7, the Bode plot of the capacitance (real part) is plotted as a function of frequency. Figure 7a,b shows the effect of $CH_3NH_3PbI_3$ crystal size and mp-TiO_2 film thickness on capacitance, respectively. As expected, C_μ is observed in the intermediate frequency (~10^2 Hz), and the C_{LF} is found near 10^{-1} Hz. In Figure 7a, C_{LF} decreases as the crystal size of $CH_3NH_3PbI_3$ increases, which indicates that less polarization is expected for the large crystal. This result is in accordance with the crystal size-dependent $I-V$ hysteresis tendency. Interestingly, however, C_μ increases with increasing crystal size, which is exactly contrary to the C_{LF} tendency. Because increase in the perovskite crystal size diminishes both the $I-V$ hysteresis and the C_{LF}, it can be suggested that C_{LF} dominantly governs the $I-V$ hysteresis rather than C_μ. This also corresponds to slow dynamic process of $I-V$ hysteresis considering that C_μ is expected to be related to the much faster kinetics in the intermediate-frequency region. Therefore, it is assumed that the relaxation time of dipole alignment or the extent of developed aligned dipole in $CH_3NH_3PbI_3$ is significantly influenced by crystal size in relation with the degree of capacitive current, which directly influences the $I-V$ hysteresis. One presumption can be carefully made in this stage that the enhancement of V_{oc} with small crystal size showing high C_{LF} is caused by not only its compact crystal morphology, preventing HTM from making direct contact with TiO_2 or FTO, but also a developed internal field inside the solar cell by the aid of highly aligned dipole, as observed in ferroelectric solar cells.[29,30] Figure 7b shows the effect of mp-TiO_2 thickness on the capacitance, where C_{LF} decreases in the presence of mp-TiO_2 and with increasing mp-TiO_2 thickness. However, C_μ is contrary to C_{LF}. This is almost the same tendency as observed in the crystal size effect. Thus, it is obvious that the suppressed $I-V$ hysteresis in the presence of mp-TiO_2 is attributed to the lowered C_{LF}, indicating that mp-TiO_2 film effectively releases polarization possibly due to the electron injection and thus charge separation.

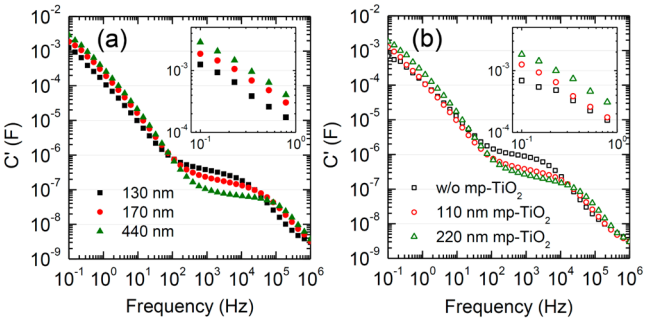

Figure 7. Bode plots of the capacitance (C', real part) obtained from impedance spectroscopy measured under one sun illumination at the applied voltage of 0.8 V for the devices with (a) different $CH_3NH_3PbI_3$ crystal size and (b) planar structure (w/o mp-TiO_2) and different mp-TiO_2 thickness. Inset shows the capacitance at low frequency (10^{-1} to 10^0 Hz).

Key parameters affecting $I-V$ hysteresis were investigated. It was found that large $CH_3NH_3PbI_3$ crystal and presence of mp-TiO_2 substantially reduced the $I-V$ hysteresis. We found that the capacitive charge would tend to be stored in smaller crystal and planar structure, which, however, released as the crystal size increased and when the mp-TiO_2 layer was employed. IS study confirmed that such $I-V$ hysteresis was related to the low-frequency capacitance that was reduced by increasing the crystal size and employing the mp-TiO_2 layer. The current study is believed to give insight into the design of the $CH_3NH_3PbI_3$ perovskite solar cell structure with minimal $I-V$ hysteresis. Nevertheless, the basis for the reduced capacitance at low frequency (C_{LF}) by increasing the perovskite size and employing the mp-TiO_2 layer is needed to be further clarified.

METHODS

Preparation of CH_3NH_3I. A mixture of hydroiodic acid (57 wt % in H_2O, Aldrich) and methylamine (40% in methanol, TCI) was stirred in the ice bath for 2 h and evaporated at 70 °C for 1 h. The resulting product was washed for 1 h with diethyl ether and filtered. To improve purity, we dissolved the product in methanol (~100 mL), and the methanol solution containing CH_3NH_3I was dropped into diethyl ether (~1000 mL). The final precipitate was filtered and dried under vacuum.

Preparation of TiO_2 Paste. Nanocrystalline anatase TiO_2 particle (average diameter = ca. 40 nm) was prepared by successive hydrolysis and hydrothermal treatment. Seed nanocrystalline anatase TiO_2 particles (average diameter = ca. 15 nm) were prepared by hydrothermal treatment of titanium isopropoxide (97%, Aldrich) at 200 °C for 12 h. The seed TiO_2 particles were added to the titanium isopropoxide solution, which was hydrothermally treated at 230 °C for 12h. The resulting TiO_2 colloidal was evaporated to remove aqueous solvent, consecutively redispersed in ethanol, and then separated using a centrifuge. The redispersion and centrifugation were repeated three times. The final TiO_2 particles dispersed in ethanol were made into a paste by adding the additives, evaporating ethanol, and mixing by a three-roll-mill. The nominal composition of the paste was TiO_2/terpineol (Aldrich)/ethylcellulose (Aldrich)/lauric acid (96%, Fluka) = 1:6:0.8:0.1.

Device Fabrication. FTO glasses (Pilkington, TEC-8, 8Ω/sq) were cleaned with a neutral detergent, followed by a sonication in a bath containing ethanol and treated in UVO cleaner for 30 min. A compact TiO_2 blocking layer was deposited on the cleaned FTO substrate by three times of spin-coating with a precursor solution containing 0.1 M titanium diisopropoxide bis(acetylacetonate) (75 wt % in 2-propanol, Aldrich) in 1-buthanol (99.8%, Aldrich). Heat treatment at 125 °C for 5 min was conducted between each spin-coating process. TiO_2 mesoporous film was spin-coated on the top of the TiO_2 compact layer using a diluted TiO_2 paste, which was annealed at 500 °C for 1 h. Film thicknesses of TiO_2 mesoporous film were controlled by spin-coating rate ranging from 500 to 3000 rpm and confirmed by a scanning electron microscope (SEM). The annealed films (flat structure and mesoporous film) were immersed in 0.02 M $TiCl_4$ (99.9%, Aldrich) aqueous for 10 min at 70 °C, which was followed by washing with DI water and heating to 500 °C for 30 min. The $CH_3NH_3PbI_3$ perovskite was formed on the prepared TiO_2 film by a sequential deposition.[3] 1 M PbI_2 (99%, Aldrich) in *N*,*N*-dimethylformamide (99.8%, Aldrich) was spin-coated and heat-treated at 70 °C for 10 min, which was immersed in a 2-propanol solution containing CH_3NH_3I and then heated finally at 100 °C for 15 min. Hole transport material (HTM) solution was composed of 56.4 mM 2,2′,7,7′-tetrakis(*N*,*N*-di-*p*-methoxyphenyl-amine)-9,99-spirobifluorene (spiro-MeOTAD, Merck), 29.9 mM bis-

dx.doi.org/10.1021/jz501392m | J. Phys. Chem. Lett. 2014, 5, 2927−2934

(trifluoromethane)sulfonimide lithium salt (Li-TFSI, 99.95%, Aldrich), and 188 mM 4-*tert*-butylpyridine (TBP, 96%, Aldrich) in the mixed solvent of chlorobenzene (99.8%, Aldrich) and acetonitrile (99.8%, Aldrich) (chlorobenzene/acetonitrile 1:0.0175 v/v). HTM solution was spin-coated on the $CH_3NH_3PbI_3$-deposited TiO_2 film. Au electrode was deposited by thermal evaporation.

Current−Voltage Measurement. Current−voltage ($I-V$) curves were measured using a solar simulator (Oriel Sol 3A class AAA) equipped with a 450 W xenon lamp (Newport 6279NS) and a Keithly 2400 source meter. One sun illumination (100 mW/cm^2) was adjusted using a silicon solar cell (NREL-calibrated) with KG-2 filter. An aperture mask was attached during the $I-V$ curve measurement. Time-dependent current was measured by a Metrohm Autolab (PGSTAT 128N) under one sun illumination, which was recorded by a General Purpose Electrochemical System (version 4.9).

Impedance Spectroscopy Measurement. Impedance spectra were measured under one sun illumination using an Autolab 302B, where bias voltage was 0.8 V. A small voltage perturbation of 30 mV was applied during the measurement at frequency ranging from 1 MHz to 0.1 Hz. The measured data were fitted using a Z-View software.

■ ASSOCIATED CONTENT

Supporting Information

Dark current−voltage curves obtained from 440 (black), 170 (red), and 130 (blue) nanometer-sized crystal of $CH_3NH_3PbI_3$. This material is available free of charge via the Internet at http://pubs.acs.org.

■ AUTHOR INFORMATION

Corresponding Author

*Tel: 82-31-290-7241. Fax: 82-31-290-7272. E-mail: npark@skku.edu.

Notes

The authors declare no competing financial interest.

■ ACKNOWLEDGMENTS

This work was supported by the National Research Foundation of Korea (NRF) grants funded by the Ministry of Science, ICT & Future Planning (MSIP) of Korea under contract nos. NRF-2010-0014992, NRF-2012M1A2A2671721, NRF-2012M3A7B4049986 (Nano Material Technology Development Program), and NRF-2012M3A6A7054861 (Global Frontier R&D Program on Center for Multiscale Energy System). H.S.K is grateful for the Global Ph.D. Fellow Grant funded by NRF. We thank Prof. Juan Bisquert from Universitat Jaume I for his comment on hysteresis phenomena.

■ REFERENCES

(1) Kim, H.-S.; Lee, C.-R.; Im, J.-H.; Lee, K.-B.; Moehl, T.; Marchioro, A.; Moon, S.-J.; Humphry-Baker, R.; Yum, J.-H.; Moser, J. E.; et al. Lead iodide Perovskite Sensitized All-Solid-State Submicron Thin Film Mesoscopic Solar Cell with Efficiency Exceeding 9%. *Sci. Rep.* **2012**, *2*, 591.

(2) Lee, M. M.; Teuscher, J.; Miyasaka, T.; Murakami, T. N.; Snaith, H. J. Efficient Hybrid Solar Cells Based on Meso-Superstructured Organometal Halide Perovskites. *Science* **2012**, *338*, 643−647.

(3) Burschka, J.; Pellet, N.; Moon, S.-J.; Humphry-Baker, R.; Gao, P.; Nazeeruddin, M. K.; Grätzel, M. Sequential Deposition as a Route to High-Performance Perovskite-Sensitized Solar Cells. *Nature* **2013**, *499*, 316−319.

(4) Liu, M.; Johnston, M. B.; Snaith, H. J. Efficient Planar Heterojunction Perovskite Solar Cells by Vapour Deposition. *Nature* **2013**, *501*, 395−398.

(5) Chen, Q.; Zhou, H.; Hong, Z.; Luo, S.; Duan, H.-S.; Wang, H.-H.; Liu, Y.; Li, G.; Yang, Y. Planar Heterojuction Perovskite Solar Cells via Vapor-Assisted Solution Process. *J. Am. Chem. Soc.* **2014**, *136*, 622−625.

(6) Ito, S.; Tanaka, S.; Manabe, K.; Nishino, H. Effects of Surface Blocking Layer of Sb_2S_3 on Nanocrystalline TiO_2 for $CH_3NH_3PbI_3$ Perovskite Solar Cells. *J. Phys. Chem. C* **2014**, *118*, 16995−17000.

(7) Leijtens, T.; Eperon, G. E.; Pathak, S.; Abate, A.; Lee, M. M.; Snaith, H. J. Overcoming Ultraviolet Light Instability of Sensitized TiO_2 with Meso-Superstructured Organometal Tri-Halide Perovskite Solar Cells. *Nat. Commun.* **2014**, *4*, 2885.

(8) Noh, J. H.; Im, S. H.; Heo, J. H.; Mandal, T. N.; Seok, S. I. Chemical Management for Colorful, Efficient, and Stable Inorganic−Organic Hybrid Nanostructured Solar Cells. *Nano Lett.* **2013**, *13*, 1764−1769.

(9) Noel, N. K.; Stranks, S. D.; Abate, A.; Weherenfennig, C.; Guarnera, S.; Haghighirad, A. A.; Sadhanala, A.; Eperon, G. E.; Johnston, M. B.; Petrozza, A. M.; et al. Lead-Free Organic-Inorganic Tin Halide Perovskites for Photovoltaic Application. *Eng. Environ. Sci.* **2014**, 10.1039/C4EE01076K.

(10) Ogomi, Y.; Morita, A.; Tsukamoto, S.; Saitho, T.; Fujikawa, N.; Shen, Q.; Toyoda, T.; Yoshino, K.; Pandey, S. S.; Ma, T.; et al. $CH_3NH_3Sn_xPb_{(1-x)}I_3$ Perovskite Solar Cells Covering up to 1060 nm. *J. Phys. Chem. Lett.* **2014**, *5*, 1004−1011.

(11) Hao, F.; Stoumpos, C. C.; Cao, D. H.; Chang, R. P. H.; Kanatzidis, M. G. Lead-Free Solid-State Organic-Inorganic Halide Perovskite Solar Cells. *Nat. Photonics.* **2014**, *8*, 489−494.

(12) Kim, H.-S.; Mora-Sero, I.; Gonzalez-Pedro, V.; Fabregat-Santiago, F.; Juarez-Perez, E. J.; Park, N.-G.; Bisquert, J. Mechanism of Carrier Accumulation in Perovskite Thin-Absorber Solar Cells. *Nat. Commun.* **2013**, *4*, 2242.

(13) Gonzalez-Pedro, V.; Juarez-Perez, E. J.; Arsyad, W.-S.; Barea, E. M.; Fabregat-Santiago, F.; Mora-Sero, I.; Bisquert, J. General Working Principles of $CH_3NH_3PbX_3$ Perovskite Solar Cells. *Nano Lett.* **2014**, *14*, 888−893.

(14) Dualeh, A.; Moehl, T.; Tétreault, N.; Teuscher, J.; Gao, P.; Nazeeruddin, M. K.; Grätzel, M. Impedance Spectroscopic Analysis of Lead-Iodide Perovskite-Sensitized Solid-State Solar Cells. *ACS Nano* **2014**, *8*, 362−373.

(15) Juarez-Perez, E. J.; Wuβler, M.; Fabregat-Santiago, F.; Lakus-Wollny, K.; Mankel, E.; Mayer, T.; Jaegermann, W.; Mora-Sero, I. Role of the Selective Contacts in the Performance of Lead Halide Perovskite Solar Cells. *J. Phys. Chem. Lett.* **2014**, *5*, 680−685.

(16) Liu, W.; Zhang, Y. Electrical Characterization of TiO_2/$CH_3NH_3PbI_3$ Heterojunction Solar Cells. *J. Mater. Chem. A* **2014**, *2*, 10244−10249.

(17) Zhoa, Y.; Zhu, K. Charge Transport and Recombination in Perovskite $(CH_3NH_3)PbI_3$ Sensitized TiO_2 Solar Cells. *J. Phys. Chem. Lett.* **2014**, *4*, 2880−2884.

(18) Bi, D.; Yang, L.; Boschloo, G.; Hagfeldt, A.; Johansson, E. M. J. Effect of Different Hole Transport Materials on Recombination in $CH_3NH_3PbI_3$ Perovskite-Sesitized Mesoscopic Solar Cells. *J. Phys. Chem. Lett.* **2013**, *4*, 1532−1536.

(19) Stranks, S. D.; Eperon, G. E.; Grancini, G.; Menelaou, C.; Alcocer, M. J. P.; Leijtens, T.; Herz, L. M.; Petrozza, A.; Snaith, H. J. Electron-Hole Diffusion Lengths Exceeding 1 Micrometer in an Organometal Trihalide Perovskite Absorber. *Science* **2013**, *342*, 341−344.

(20) Xing, G.; Mathews, N.; Sun, S.; Lim, S. S.; Lam, Y. M.; Grätzel, M.; Mhaisalkar, S.; Sum, T. C. Long-Range Balanced Electron-and Hole-Transport Lengths in Organic-Inorganic $CH_3NH_3PbI_3$. *Science* **2013**, *342*, 344−347.

(21) Umari, P.; Mosoconi, E.; Angelis, F. D. Relativistic GW Calculations on $CH_3NH_3PbI_3$ and $CH_3NH_3SnI_3$ Perovskites for Solar Cell Applications. *Sci. Rep.* **2014**, *4*, 4467.
(22) Edri, E.; Kirmayer, S.; Mukhopadhyay, S.; Gartsman, K.; Hodes, G.; Cahen, D. Elucidating the Charge Carrier Separation and Working Mechanism of $CH_3NH_3PbI_{3-x}Cl_x$ Perovskite Solar Cells. *Nat. Commun.* **2014**, *5*, 3461.
(23) Snaith, H. J.; Abte, A.; Ball, J. M.; Eperon, G. E.; Leijtens, T.; Noel, N. K.; Stranks, S. D.; Wang, J. T.-W.; Wojciechowski, K.; Zhang, W. Anomalous Hysteresis in Perovskite Solar Cells. *J. Phys. Chem. Lett.* **2014**, *5*, 1511−1515.
(24) Herman, M.; Jankovec, M.; Topič, M. Optimal I-V Curve Scan Time of Solar Cells and Modules in Light of Irradiance Level. *Int. J. Photoenergy* **2012**, *2012*, 151452.
(25) Koide, N.; Han, L. Measuring Methods of Cell Performance of Dye-Sensitized Solar Cells. *Rev. Sci. Instrum.* **2004**, *75*, 2828−2831.
(26) Sanchez, R. S.; Gonzalez-Pedro, V.; Lee, J.-W.; Park, N.-G.; Kang, Y. S.; Mora-Sero, I.; Bisquert, J. Slow Dynamic Process in Lead Halide Perovskite Solar Cells. Characteristic Times and Hysteresis. *J. Phys. Chem. Lett.* **2014**, *5*, 2357−2363.
(27) Friesen, G.; Ossenbrink, H. A. Capacitance Effects in High-Efficiency Cells. *Sol. Energy Mater. Sol. Cells* **1997**, *48*, 77−83.
(28) Juarez-Perez, E. J.; Sanchez, R. S.; Badia, L.; Garcia-Belmonte, G.; Kang, Y. S.; Mora-Sero, I.; Bisquert, J. Photoinduced Giant Dialectic Constant in Lead Halide Perovskite Solar Cells. *J. Phys. Chem. Lett.* **2014**, *5*, 2390−2394.
(29) Yang, S. Y.; Seidel, J.; Byrnes, S. J.; Shafer, P.; Yang, C.-H.; Rossell, M. D.; Yu, P.; Chu, Y.-H.; Scott, J. F.; Ager, J. W.; et al. Above-Bandgap Voltages from Ferroelectric Photovoltaic Devices. *Nat. Nanotechnol.* **2010**, *5*, 143−147.
(30) Seidel, J.; Fu, D.; Yang, S.-Y.; Alarcón-Lladó, E.; Wu, J.; Ramesh, R.; Ager, J. W. Efficient Photovoltaic Current Generation at Ferroelectric Domain Walls. *Phys. Rev. Lett.* **2011**, *107*, 126805.